Article

Preparation and Characterization of Oxide Nanotubes on Titanium Surface for Use in Controlled Drug Release Systems

Patrycja Osak *, Sandra Skwarek, Dariusz Łukowiec, Grzegorz Przeliorz, Bożena Łosiewicz *

Posted Date: 24 June 2024

doi: 10.20944/preprints202406.1645.v1

Keywords: anodizing; corrosion resistance; drug delivery system; oxide nanotubes; titanium

 doi:10.20944/preprints202406.1645.v1

Article

Preparation and Characterization of Oxide Nanotubes on Titanium Surface for Use in Controlled Drug Release Systems

Patrycja Osak [1,*], Sandra Skwarek [1], Dariusz Łukowiec [2], Grzegorz Przeliorz [3] and Bożena Łosiewicz [1,*]

[1] University of Silesia in Katowice , Faculty of Science and Technology, Institute of Materials Engineering, 75 Pułku Piechoty 1A, 41-500 Chorzów, Poland; sandraskwarek99@gmail.com (S.S.)
[2] Silesian University of Technology, Faculty of Mechanical Engineering, Konarskiego 18a, 44-100 Gliwice, Poland; Dariusz.Lukowiec@polsl.pl (D.L.)
[3] COMEF, Gdańska 2, 40-719 Katowice, Poland; grzegorz.przeliorz@comef.com.pl (G.P.)
* Correspondence: patrycja.osak@us.edu.pl (P.O.); Tel.: +48-32-3497-524; bozena.losiewicz@us.edu.pl (B.Ł.); Tel.: +48-32-3497-527

Abstract: Preventing or treating infections at implantation sites where the risk of bacterial contamination is high requires the development of intelligent drug delivery systems. In this work, honeycomb structures as a potential drug carrier were obtained for the first time in a fast, one-step anodization process of titanium grade 4, lasting only 60 seconds. Fourth generation oxide nanotube layers were obtained from an aqueous solution of 0.5% $AgNO_3$ in the voltage range from 50 to 80 at 15(1) °C. The FE-SEM method showed the length of the oxide nanotubes from 1.02(2) μm at 50 V to 230(8) nm at 80 V. The EDS analysis revealed that during anodizing, silver particles are deposited on the Ti G4 up to 2.2(5) wt.%. Electrochemical measurements by open circuit potential and anodic polarization curves methods proved the improvement of in vitro corrosion resistance as a result of Ti G4 anodizing. Assessment of the anodized Ti G4 as gentamicin sulfate carrier carried out using ATR-FTIR and UV-VIS absorption spectroscopy revealed that the obtained oxide nanotube layers can be used for application of drugs directly to the tissue around the implant. This method of application allows full use of the therapeutic dose of the antibiotic used.

Keywords: anodizing; corrosion resistance; drug delivery system; oxide nanotubes; titanium

1. Introduction

Titanium is characterized by biotolerance in the human body [1]. This metal also has low density, high corrosion resistance and the ability to osseointegrate. Titanium is a vital element, which means that it does not have any harmful effects on the human body. Implants made of titanium are characterized by a long durability of 15 to 20 years. The constantly increasing number of toothless people and the desire to ensure the comfort of life lead to more frequent implantation of dental implants made of titanium. However, the use of titanium implants does not fully meet the needs of modern medicine [1,2].

Surface treatment of dental implants increases the bioactivity of titanium implants [3,4]. Implantology also strives to use intelligent drug delivery systems (DDSs). Appropriate selection of surface treatment ensures the desired clinical effects. Surface treatment technologies are evolving very quickly. The anodized surface is best suited for use as drug carriers. This process is used in pharmacology, materials science and biomedical engineering. In the anodizing process, a porous surface or one with oxide nanotubes can be obtained. Studies have shown that using the anodizing process does not leave harmful incompatible elements on the surface [3–5]. Additionally, anodizing is a simple, cheap and easily scalable method that allows obtaining oxide nanotubes with an ordered structure. Layers of oxide nanotubes on the titanium surface increase the substrate's ability to mineralize bone tissue thanks to the developed surface and increased roughness.

 doi:10.20944/preprints202406.1645.v1

Oxide nanotubes on titanium and its alloys are most often obtained in fluorine-based electrolytes [6]. Depending on the generation of the oxide nanotubes produced, by changing the current-time parameters and the amount of fluoride ions, nanotubes of various lengths and diameters can be obtained. Current trends aim to use reagents in the spirit of green chemistry, limiting the use of fluoride ions, which is why the fourth generation of oxide nanotubes is obtained in fluoride-free electrolytes. This type of electrochemical oxidation is characterized by the rapid growth of oxide nanotubes that are several microns long and lack order. The most commonly used electrolytes in the anodic production of fourth-generation oxide nanotubes are based on HCl [7,8], H_2O_2 [8,9] and their aqueous solutions, as well as mixtures of oxalic acid [10], formic acid [10], and sulfuric acid [11]. Fourth-generation oxide nanotubes are also obtained from aqueous solution of $AgNO_3$ [12], $SrNO_3$, $NaNO_3$, and KNO_3 [13]. The mechanism for obtaining oxide nanotubes from non-fluoride solutions is different than in the case of baths containing fluoride ions. After applying the appropriate voltage to the electrode, the anode current density increases rapidly and reaches its maximum values very quickly. The thickness of the obtained oxide reaches its maximum value immediately after the process starts, followed by an avalanche of breakdown and intensive oxygen evolution [12].

In the case of layers of oxide nanotubes obtained from nitrate baths, especially silver nitrate, along with obtaining a layer of oxide nanotubes, it is also possible to incorporate Ag particles inside the obtained nanotube structures during the anodizing process [12]. Silver is famous for its antibacterial properties, so it can be used in the treatment of peri-implantation infections, in particular *Staphylococcus aureus* [12,14,15], which is the most common cause of implant loss. Currently, the addition of silver nanoparticles is used as a bactericidal agent in medicine, as well as in disinfectants [16].

This work was undertaken to carry out innovative surface functionalization of titanium Garde 4 (Ti G4) by creating fourth-generation nanotubular oxide layers. The chosen method of modifying the Ti G4 surface by anodizing was aimed at shaping the surface morphology, structure and properties for applications in intelligent DDSs. The first stage was the selection of voltage, time and type of electrolyte. In the second stage, the physico-chemical characterization of the obtained anode layers was carried out using field emission scanning electron microscopy (FE-SEM), energy dispersive spectroscopy (EDS) and Furier transform infrared spectroscopy (FTiR). The third stage was to determine the mechanism and kinetics of the release of the drug substance in the form of gentamicin sulfate from the obtained oxide nanotubes based on UV-VIS analysis. GS is a broad-spectrum antibiotic, effective against a wide range of Gram-negative bacteria [17]. This makes it a valuable choice for preventing or treating infections at implant sites, where the risk of bacterial contamination is high. It is highly potent, meaning that even small amounts can be effective against bacteria. This is particularly beneficial when loading drugs into porous layers, as it allows for the effective use of the available space and material.

2. Materials and Methods

2.1. Substrate Preparation

The material used as an anodizing substrate was Ti G4 (Bibus Metals, Dąbrowa, Poland) in the form of a rod with a diameter of 10 mm and a length of 1500 mm after cold forming to increase mechanical properties and, in particular, strength. Ti G4 rods met the requirements of ISO 5832-2:2018-08: Implants for Surgery - Metallic Materials - Part 2: Unalloyed Titanium and ASTM F67-13: Standard Specification for Unalloyed Titanium, for Surgical Implant Applications (UNS R50250, UNS R50400, UNS R50550, UNS R50700). The tested samples were prepared in the form of 5 mm thick discs and then wet polished on silicon carbide abrasive papers of various gradations in increasing grit 600, 800, 1200, 3000 and 5000 using the metallographic grinding and polishing machine Metkon Forcipol 102 (Metkon Instruments Inc., Bursa, Turkey). After polishing each sample was washed for 20 min in ultrapure water with a resistivity of 18.2 MΩ cm at a temperature of 25 °C (Milli-Q® Advantage A10 Water Purification System, Millipore SAS, Molsheim, France) using the USC 300 TH ultrasonic cleaner (VWR International, Radnor, PA, USA), ensuring effective removal of

 doi:10.20944/preprints202406.1645.v1

contaminants from elements with complex geometry. The washing procedure in ultrapure water was repeated twice.

2.2. Anodizing Conditions of Ti G4

For the anodizing process, electrodes were made from polished Ti G4 by attaching an insulated copper wire to the back of the titanium samples using silver glue to ensure electrical contact. The back side of the alloy samples and the side walls were protected with chemically resistant two-component epoxy resin. The electrodes were then cleaned with Milli-Q® water in an ultrasonic bath for 20 minutes and placed in the bath for the anodizing process in a two-electrode system. Anodizing was performed in an aqueous solution of 0.5% silver nitrate (Sigma-Aldrich, Saint Louis, Missouri, USA) at a thermostated temperature of 15(1)°C at a voltage of 50 to 80 V for 60 seconds. Anodizing was carried out using a high-current PWR800H power supply (Kikusui Electronics Corporation, Yokohama, Japan). The distance of the sample (anode) with a geometric area of 0.64 cm^2 from the platinum mesh (cathode) with an area of 16 cm^2 was constant and amounted to 20 mm. After the anodizing process, the electrodes were rinsed in Milli-Q® water and air-dried at ambient temperature.

2.3. FE-SEM Measurements

The surface morphology and thickness of the oxide nanotube layers on the Ti G4 surface were examined using a Hitachi HD-2300A field emission scanning electron microscope (FE-SEM) (Hitachi Ltd., Tokyo, Japan) under a low vacuum condition of 50 Pa at an accelerating voltage of 15 kV and using a Hitachi TM4000/TM4000Plus II microscope - Hitachi High Technologies (Hitachi Ltd., Tokyo, Japan) under low vacuum conditions at an accelerating voltage of 20 kV. All microscopic images were collected by secondary electrons (SE). The local chemical composition and surface distribution of elements were determined using an Energy Dispersive Spectrometer (EDS, AZtecLiveOne 30mm^2 Oxford Instruments, Abingdon, Great Britain).

2.4. ATR-FTIR Measurements

Fourier attenuated total reflectance infrared spectroscopy (ATR-FTIR) was used to determine the functional groups of the obtained oxide nanotubes before and after antibiotic implementation. Radiation covering the infrared range from 4000 to 550 cm^{-1} was split into two beams, one of which followed a path of a fixed length, and the other was generated by an interferometer with a moving mirror moving at a constant speed. The changing difference in the path lengths of both beams caused mutual interference, resulting in an interferogram. The use of the Fourier transform allowed the interferogram to be transformed from the time domain to the frequency domain, i.e. spectrum. Transmittance measurements in the fundamental infrared range were based on the phenomenon of total internal reflection of light from the interface of two materials with different refractive indices. ATR-FTIR absorption spectra were recorded using a Shimadzu IR Prestige-21 FTIR spectrophotometer (Shimadzu, Kyoto, Japan) equipped with an ATR reflectance adapter with a diamond.

2.5. In Vitro Corrosion Resistance in Artificial Saliva Solution

The in vitro corrosion resistance test of the obtained electrodes was carried out in artificial saliva solution (ASS) with pH = 7.4(1) at a temperature of 37(1) °C. ASS consisted of NaCl – 0.70 g dm^{-3}, KCl – 1.20 g dm^{-3}, Na_2HPO_4 – 0.26 g dm^{-3}, $NaHCO_3$ – 1.50 g dm^{-3} and KSCN – 0.33 g dm^{-3}. A 4% NaOH solution and a 1% $C_3H_6O_3$ solution were used to adjust the pH. Immediately before the measurements, a fresh portion of the solution was deaerated in 99.9999% pure argon (Air Liquide S.A., Paris, France) for 20 min.

All electrochemical studies were performed using a computer-controlled ModuLab XM ECS electrochemical system (Solartron Analytical, Farnborough, UK). Electrochemical measurements were carried out in a three-electrode system consisting of a working electrode (WE) in the form of the tested material, a counter electrode (CE) made of a platinum mesh, and a reference electrode (RE)

 doi:10.20944/preprints202406.1645.v1

placed in the Luggin capillary against which all potential values were measured. The reference electrode was a saturated calomel electrode (SCE) with a potential of 244.4(1) mV.

In vitro tests of the corrosion resistance of the obtained electrodes began with the measurement of the open circuit potential (E_{OC}). According to ISO 10271:2021-02: Dentistry - Corrosion Test Methods for Metallic Materials, the measurement time for the E_{OC} change was 2 hours with a sampling frequency of every 10 seconds. In E_{OC} measurements, the zero current galvanostatic potentiometry method with physical disconnection of CE was used. The obtained $E_{OC} = f(t)$ curves were used for a preliminary assessment of the corrosion resistance of the tested electrodes. The stabilized E_{OC} value was considered as an approximate value of the corrosion potential (E_{cor}) in further electrochemical tests.

The susceptibility to pitting corrosion was tested using anodic polarization curves in accordance with the ISO 10271:2022-02 standard: Dentistry - Corrosion Test Methods for Metallic Materials. The measurement was carried out from a potential of 150 mV more negative relative to the E_{OC} towards the anode potentials, recording the cathode-anode transition up to a potential of 4 V. Three measurement series were performed for each type of electrode, and the determined parameter values were given as average values with standard deviation (SD).

2.7. Gentamicin Sulfate Loading and Release from Oxide Nantubes on Ti G4

Fourth-generation oxide nanotube layers obtained on the Ti G4 surface were used as a drug carrier with controlled release of the drug substance. The drug release kinetics studies used an antibiotic in the form of gentamicin sulfate (GS) with the formula $C_{60}H_{127}N_{15}O_{26}S$ (Merck KGaA, Darmstadt, Niemcy).

The anodized Ti G4 samples were immersed in 7 ml of drug solution (50 mg mL^{-1}). The initial drug dose was 350 mg for each sample. A Ti G4 sample with oxide nanotubes produced at a voltage of 50 to 60 V and a time of 60 seconds was immersed in the solution prepared in this way for 24 hours. After 24 hour, 1.5 mL of the solution containing GS was taken and the amount of drug absorbed inside the oxide nanotubes was determined.

The amount of the absorbed drug was determined using the UV-VIS absorption spectroscopy method using electromagnetic radiation in the visible light (VIS) and near ultraviolet (UV) range. The work used a UV-Vis Biowave 2 (Biochrom WPA Biowave II UV/Visible Spectrophotometer, Cambridge, England) spectrophotometer equipped with diode-array optics, enabling precise measurements with an open measurement chamber. The absorbance value was measured at a wavelength of $\lambda = 245$ nm, determining in the first step the absorbance value of the drug solution and then the absorbance value of the collected solution after drug implementation.

The release kinetics of GS implemented inside the oxide nanotubes was examined by immersing the sample in 15 mL of phosphate buffer solution (PBS) at pH = 7.4(1) at 37 °C for 5 days. During the first hour, PBS was collected for analysis every hour, then every 24 hours for 5 days. Each time, 1 mL of PBS was collected and fresh solution was added. The amount of drug substance released from the oxide nanotubes was determined by UV-Vis spectroscopy. The absorbance was measured at a wavelength of $\lambda = 250$ nm, in the first stage determining the absorbance value of PBS and then the absorbance of the tested solution. The amount of GS released in percent by weight was determined from the drug calibration curve.

3. Results and Discussion

3.1. Formation of Oxide Nanotubes on Ti G4

The course of current densities as a function of time for Ti G4 electrodes anodized in a 0.5% $AgNO_3$ solution is shown in Figure 1. It can be observed that as the voltage used in the anodizing process increases, the current density increases. The characteristic trough is not visible on the recorded curves $j = f(t)$, resulting from the formation of oxide nanotubes of the first to third generation due to the presence of fluoride ions in the bath [18]. In the case of a fluoride-free bath, a sharp increase

 doi:10.20944/preprints202406.1645.v1

in current density is visible, as in Figure 1. This increase is caused by the fact that the emerging oxide film is produced as a result of the dissolution of oxides, which begins at the electrolyte | oxide [19].

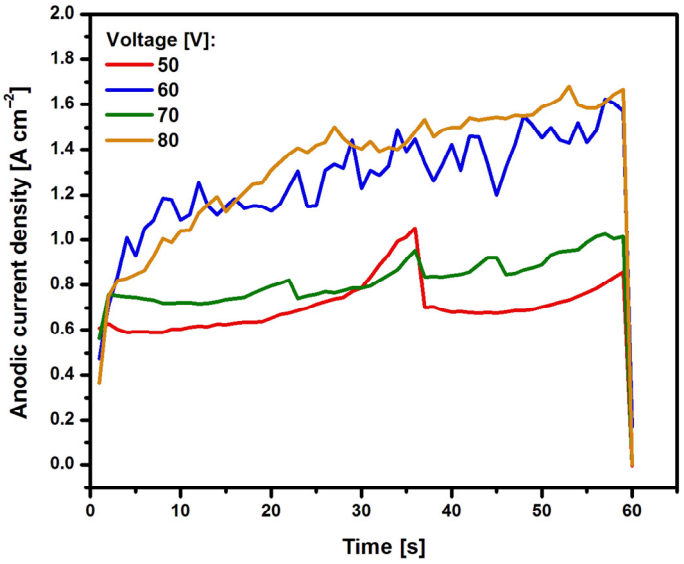

Figure 1. Dependence of current density (j) on time (t) for the Ti G4 electrode in 0.5% $AgNO_3$ solution during anodizing at voltage from 50 to 80 V for 60 s.

In the anodizing process in a fluoride-free bath, immediately after the start of electrochemical oxidation, the oxide layer is rapidly broken down, generating oxygen gas and a high current density value. Bauer et al. in [20] suggest that the oxide formed on the titanium surface has no resistivity, hence a high current can flow through the formed layer after reaching the breakdown voltage. During anodizing, the following electrochemical reactions occur in a fluoride-free solution [12]:

$$Ti \rightarrow Ti^{4+} + 4e^{-}, \quad (1)$$

$$2H_2O \rightarrow O_2 \uparrow + 4H^{+} + 4e^{-}. \quad (2)$$

In the process of anodic production of oxide nanotubes, a number of reactions occur in parallel. Reactions mainly take place at the interface between metal|oxide and metal|electrolyte phases [21–23]. Figure 2 shows a diagram of the formation of oxide nanotubes on the surface of titanium covered with a barrier layer, i.e. a self-passive TiO_2 oxide layer. During the anodizing process, a constant voltage current flows through the electrode. As a result of anodizing, the thin and self-passive barrier layer thickens (Figure 2, I) [21]. With the time of the anodizing process, the electrical resistance of the system increases and the thickness of the oxide increases, which cracks (Figure 2, II) [21]. Then, the thick barrier layer further breaks down, facilitating the penetration of the electrolyte inside, and a porous structure is formed (Figure 2, III) [21]. Then, stabilization and formation of nanotubes/nanopores on the surface of the material is observed (Figure 2, IV) [21].

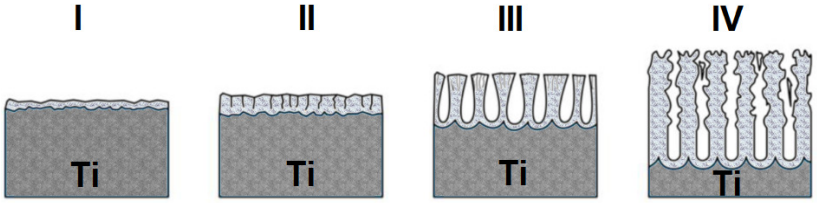

Figure 2. Scheme of anodic production of oxide nanotubes from a fluoride-free bath on the titanium surface: I – barrier layer, II – increase in the thickness of the barrier layer and the formation of cracks, III – formation of a porous structure, IV – production of oxide nanotubes.

 doi:10.20944/preprints202406.1645.v1

The anodizing process takes place in three stages [19,24,25]. During the electrochemical oxidation process, a very rapid release of bubbles from the anode surface is visible. In the anodizing process, an ionic current (j_i) and an electronic current (j_e) are generated [24]. J_i is responsible for the formation of oxide, and j_e is responsible for the formation of oxygen gas [12,24]. Oxide formation on the electrode surface influences the formation of the nanotube wall (Equation 1), and oxygen evolution influences the nanotube to remain open (Equation 2). As the anodizing voltage applied increases, the amount of released oxygen gas increases and, consequently, the current density increases. During the anodizing process, the thickness of the barrier layer increases, and when it approaches the critical thickness, a high current density value is generated and the current value j_i decreases [19]. At the same time, a strong evolution of O_2 gas begins at the boundary of the oxide film on the electrolyte side [25]. In the second stage, air bubbles accumulate on the electrode surface, creating the beginning of the formation of nanotubes. In the third stage, oxygen gas escapes from the interior of the oxide nanotubes, facilitating the electrolyte to reach the interior of the nanotubes. At the end of the production of nanotubes, the value of the current density decreases to a state close to zero [12,19,25].

3.2. FE-SEM/EDS Characterization of Oxide Nanutubes on TiG4

Based on FE-SEM images, the morphology and length of oxide nanotubes obtained on the Ti G4 surface under the proposed anodizing conditions were determined (Figure 3). The obtained microscopic images show an even distribution of single-wall oxide nanotubes. Each of the appropriately selected anodizing voltages ensured the production of fourth-generation oxide nanotubes.

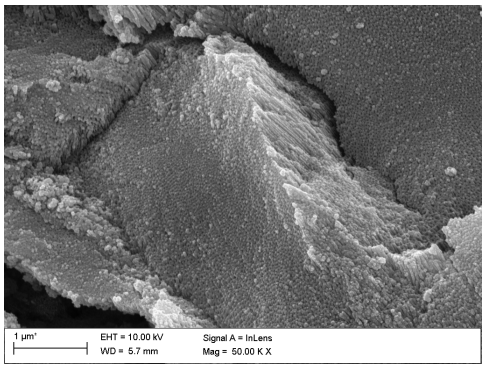

(**a**)

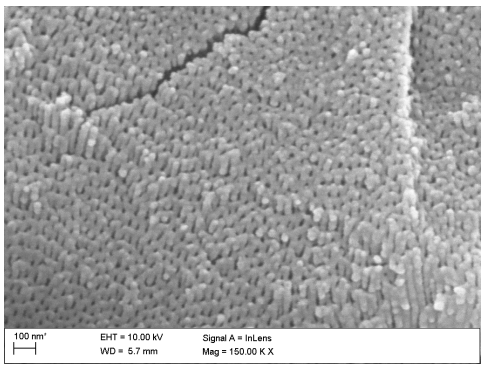

(**b**)

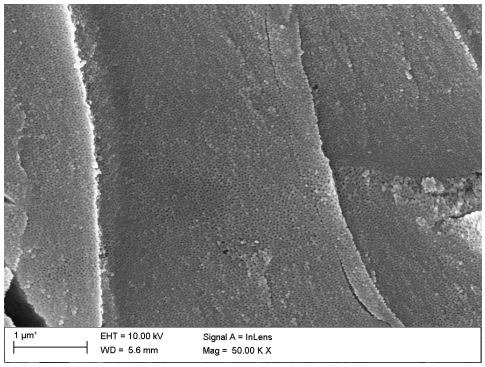

(**c**)

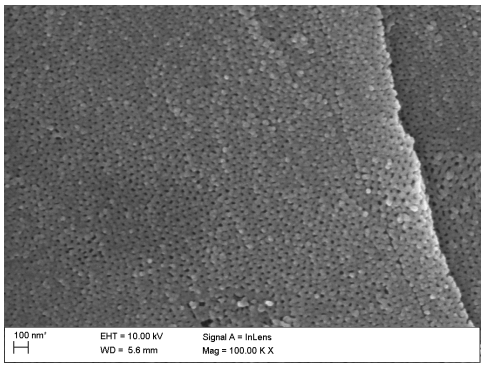

(**d**)

 doi:10.20944/preprints202406.1645.v1

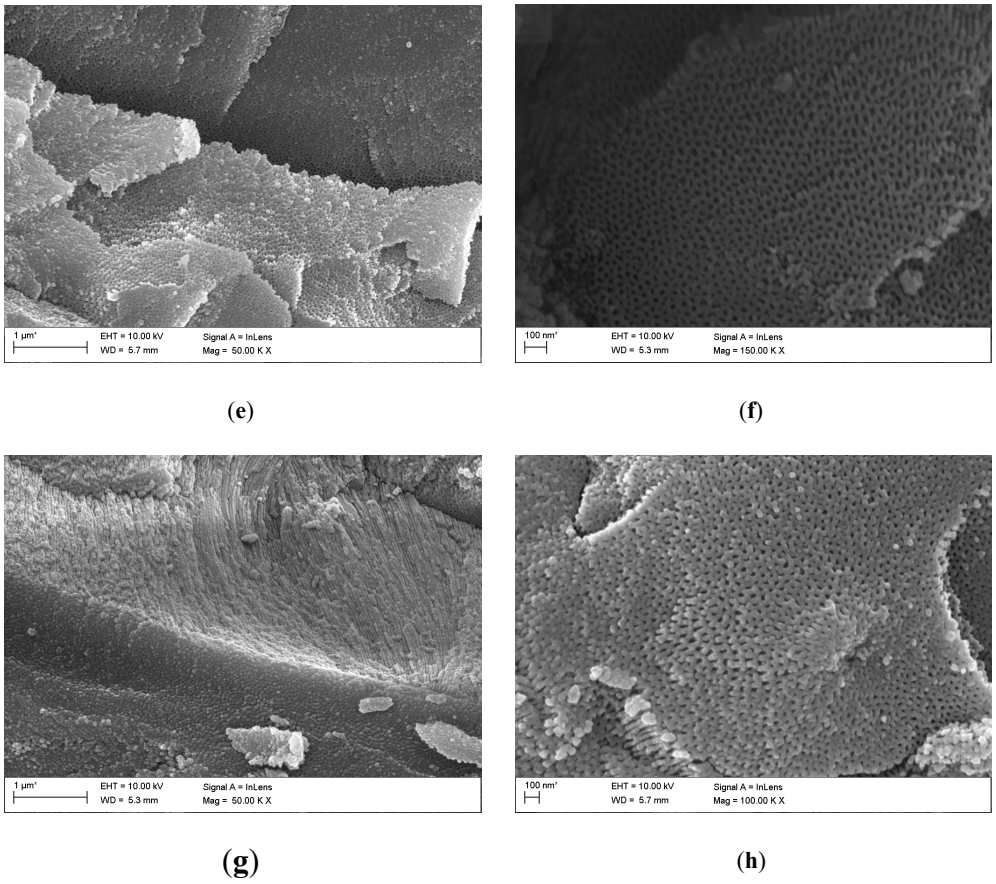

Figure 3. FE-SEM image of the microstructure of oxide nanotubes obtained on the Ti G4 surface by anodizing for 60 seconds at the voltage: (**a**)–(**b**) 50 V; (**c**)–(**d**) 60 V; (**e**)–(**f**) 70 V; (**g**)–(**h**) 80 V.

Based on FE-SEM images, the length of oxide nanotubes was determined to be approximately 1.0(2) µm for the anodized surface at a voltage of 50 V, approximately 550(13) nm at a voltage of 60 V, approximately 375(11) nm at a voltage of 70 V and approximately 230(8) nm at 80 V. On this basis, it can be concluded that as the anodizing voltage increases, the length of the obtained nanotubes decreases. After anodizing, each surface shows a honeycomb structure and multi-layer surfaces [26]. At a voltage of 50 V, nanopores/nanotubes formed, but their pores are clogged in some places with the remains of the oxide layer, which did not transform into nanotubes (Figure 3a,b). At a voltage of 60 V (Figure 3c and d) and 70 V (Figure 3e and f), no remnants of the unoxidized oxide film are observed on the surface of the oxide nanotubes. Figure 3g and h indicates that increasing the voltage to 80 V resulted in the formation of regular pores with a hexagonal structure [26,27]. In the literature, this type of structure is obtained by two-stage anodic oxidation in acidic solutions [26,28,29]. In this work, honeycomb structures were obtained in a fast, one-step anodization process, lasting only 60 seconds. The hexagonal structure is used when nanotubes are used as carriers in intelligent drug delivery systems [27,29].

The use of $AgNO_3$ solution in the Ti G4 anodizing process enabled not only the formation of layers of fourth-generation oxide nanotubes, but also the co-deposition of silver particles. Figure 4 shows an example of the surface distribution of elements in the tested micro-area on the Ti G4 surface after the anodizing process at a voltage of 80 V. A uniform distribution of elements such as titanium, oxygen and silver in the examined micro-area on the surface of the obtained layer of oxide nanotubes is visible.

 doi:10.20944/preprints202406.1645.v1

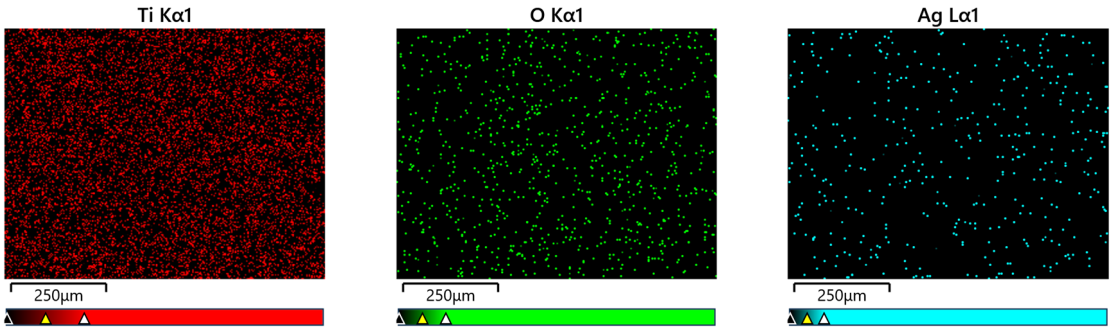

(**a**) (**b**) (**c**)

Figure 4. Map of the surface distribution of elements on the Ti G4 surface after anodizing in 0.5% $AgNO_3$ solution at a voltage of 80 V: (**a**) Ti; (**b**) O; (**c**) Ag.

The amount of silver on the surface of all oxide nanotube layers obtained on a Ti G4 substrate was determined by EDS microanalysis. An example FE-SEM image of the tested micro-areas on the Ti G4 surface after anodizing in 0.5% $AgNO_3$ solution at a voltage of 50 V is and the recorded EDS spectrum is shown in Figure 5a and b, respectively. EDS analysis showed that by oxidizing Ti G4 at voltages of 50 and 60 V, approximately 1.4(2) wt.% Ag was incorporated into the anodized surface (Table 1). The increase in anodizing voltage increases the amount of silver in the oxide layer, which is 1.9(1) wt.% at 70 V and 2.2(5) wt.% at a voltage of 80 V (Table 1).

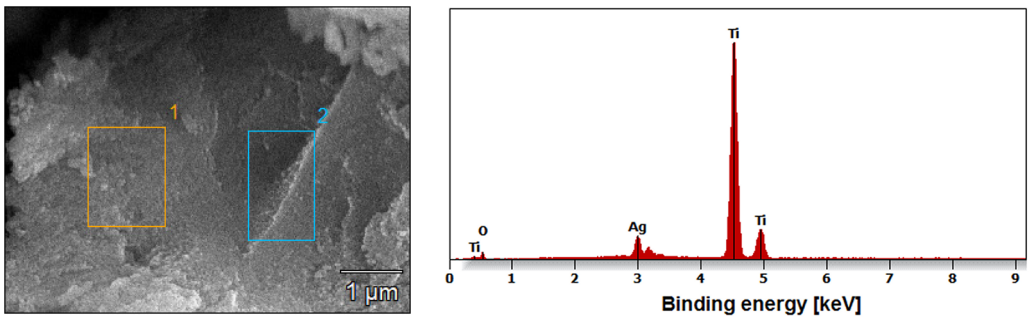

(**a**) (**b**)

Figure 5. Micro-areas on the Ti G4 surface after anodizing in 0.5% $AgNO_3$ solution at 50 V for 60 seconds: (**a**) FE-SEM image; (**b**) EDS spectrum.

Table 1. Quantitative analysis of elements present on the surface of oxide nanotube layers obtained on a Ti G4 substrate in a 0.5% $AgNO_3$ solution.

Voltage [V]	Element [wt.%]		
	O	Ti	Ag
50	35.8(2)	62.8(4)	1.4(2)
60	38.1(1)	61.5(2)	1.4(1)
70	25.0(7)	73.0(3)	1.9(1)
80	30.9(2)	66.9(1)	2.2(5)

It should be noted that the presence of silver influences interactions with the bacterial structures of the biofilm that appears in the oral environment [30]. Using electrostatic forces, silver particles are attracted to the cytoplasmic membrane and the cell membrane wall. As a consequence, the membrane becomes semi-permeable and destroys bacterial structures [31]. The silver particles present in the oxide nanotube layer are small, so they have a positive effect on inhibiting bacteria after the implantation process. Too high a content of silver present on the surface may influence changes in the DNA structure and induce oxidative stress and genotoxicity [32].

 doi:10.20944/preprints202406.1645.v1

Local measurement of the chemical composition of the tested materials using the microanalytical EDS method also showed the presence of titanium and oxygen. However, it should be emphasized that determining the percentage of oxygen using this method is difficult due to the fact that the characteristic radiation of light elements is absorbed more intensively by the sample. Moreover, atoms from ^{5}B to ^{10}Ne have only two shells filled with electrons, i.e. only one K emission series. The excitation energy of the K series is therefore very small and amounts to a maximum of 1 keV [33].

3.3. Assessment of In Vitro Corrosion Resistance in Artificial Saliva Solution

3.3.1. Open Circuit Potential Study

Figure 6 shows the relationship of the open circuit potential on the immersion time in ASS at 37 °C for the Ti G4 electrode before and after anodizing at 50 to 80 V for 60 seconds in 0.5% silver nitrate solution. The obtained $E_{OC} = f(t)$ curves were used for a preliminary assessment of the in vitro corrosion resistance of the tested electrodes.

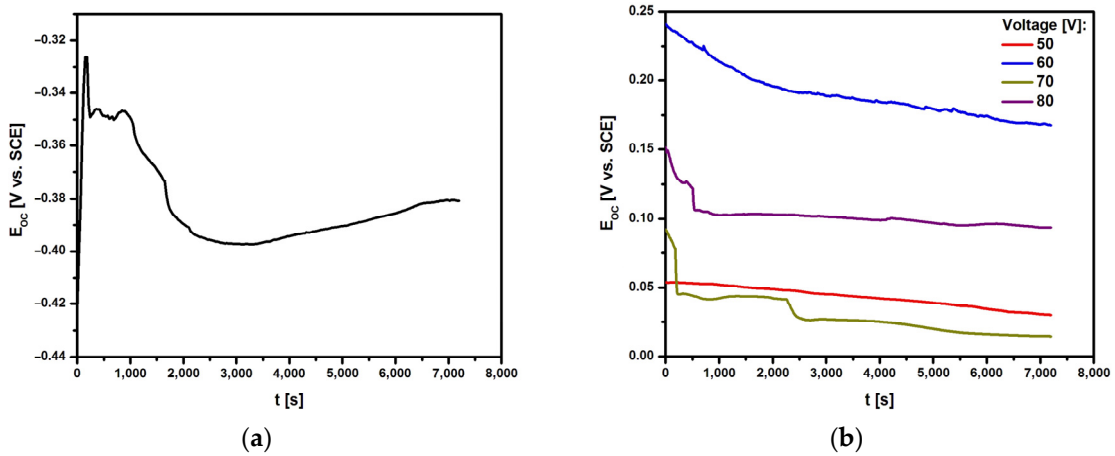

(**a**) (**b**)

Figure 6. Dependence of the open circuit potential (E_{OC}) on the immersion time (t) in artificial saliva solution at 37 °C for the Ti G4 electrode: (**a**) After mechanical polishing; (**b**) After anodizing at 50 to 80 V for 60 seconds in 0.5% silver nitrate solution.

For all tested electrodes, the E_{OC} value changed dynamically in the first 2,000 seconds. Ion-electron equilibrium, manifested by a stable E_{OC} value, was achieved after 7,200 seconds. The E_{OC} for the mechanically polished Ti G4 electrode is –0.381(4) V (Figure 6a). The use of surface modification by anodizing at voltages from 50 to 80 V shifts the E_{OC} value towards positive potentials at which the electrochemical oxidation process is more difficult (Figure 6b). The stable E_{OC} value is between 0.015(3) and 0.168(8) V depending on the anodizing voltage. Such a nature of the $E_{OC} = f(t)$ curves indicates an increase in the corrosion resistance of Ti G4 as a result of the surface modification and improvement of the barrier properties of the oxide layer as a result of its thickening.

3.3.2. Anodic Polarization Curves Study

The susceptibility of the Ti G4 electrode to pitting corrosion in ASS containing aggressive chloride ions at a temperature of 37 °C was tested in the initial state, i.e. after mechanical polishing (0 V) and after anodizing at a voltage of 50 to 80 V for 60 seconds in 0.5% silver nitrate solution based on anodic polarization curves. During the measurement, the change in the potential of the tested electrodes was recorded using an electrode polarization rate of $v = 1$ mV s^{-1}. The recorded anodic polarization curves are presented in the semi-logarithmic form $\log|j| = f(E)$ in Figure 7.

 doi:10.20944/preprints202406.1645.v1

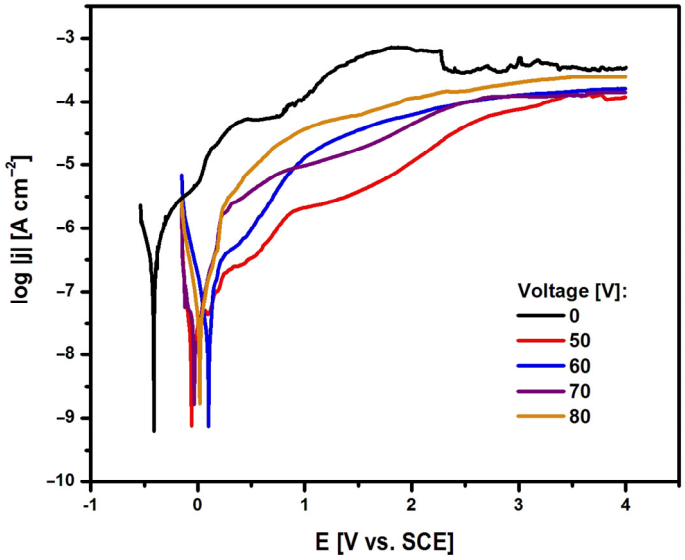

Figure 7. Anodic polarization curves for the Ti G4 electrode before and after anodizing at 50 to 80 V for 60 seconds in 0.5% silver nitrate solution, obtained in ASS at a temperature of 37 °C.

Based on the results obtained, it can be seen that the use of surface modification by creating layers of fourth-generation oxide nanotubes increases the corrosion resistance of Ti G4. Potentiodynamic characteristics for oxide nanotube layers obtained on the Ti G4 surface in the voltage range from 50 to 80 V for 60 seconds in a 0.5% $AgNO_3$ solution show a similar course. The lowest value of E_{cor} = –0.412(16) V, indicating the lowest corrosion resistance, was obtained for the Ti G4 surface before anodization with a self-passive oxide layer on the surface. In the case of the Ti G4 surface anodized at 50 V, the E_{cor} value is –0.059(7) V, at 60 V the E_{cor} is equal to 0.099(10) V, at 70 V E_{cor} takes a value of –0.035(9) V, and at 80 V E_{cor} is 0.018(8) V. The highest average j_{cor} value of approximately 3.39×10^{-7} A cm^{-2} is observed for the Ti G4 electrode after mechanical polishing, indicating the fastest kinetics of the corrosion process. The average j_{cor} value for the oxide nanotube layer obtained at 50 and 60 V is 7.59×10^{-10} A cm^{-2} and 7.36×10^{-10} A cm^{-2}, respectively. For oxide nanotube layers obtained at higher voltages, i.e. 70 and 80 V, j_{cor} value is 1.35×10^{-9} A cm^{-2} and 1.67×10^{-9} A cm^{-2}, respectively. The tested Ti G4 electrodes with oxide layers on the surface show corrosion resistance in the range of cathodic potentials and passive anodic behavior. In the range of anodic potentials, electrochemical oxidation reactions occur at values that are more positive compared to E_{cor}. The obtained potentiodynamic characteristics confirm that the anodizing process of Ti G4 under the proposed electrochemical conditions increases the in vitro corrosion resistance of Ti G4, which can be used for long-term implants. Similar behavior was observed in the literature for titanium and its alloys covered with oxide layers in biological environments [34–37].

3.4. Assessment of Oxide Nanotube Layers on Ti G4 as Drug Carriers

3.4.1. ATR-FTIR Characterization of Anodized Ti G4 After GS Implementation

To assess the possibility of using the obtained layers of oxide nanotubes on a Ti G4 substrate as a potential drug carrier for applications in intelligent drug DDSs, gentamicin sulfate was implemented inside the nanotubes. ATR-FTIR characterization was performed on Ti G4 samples after anodization in 0.5% $AgNO_3$ solution at 50, 60, 70 and 80 V for 60 seconds with absorbed drug and, comparatively, on gentamicin sulfate in the initial state in the form of powder (Figure 8). Based on the ATR-FTIR spectroscopic measurements, individual functional groups were assigned to specific areas with characteristic absorption bands.

 doi:10.20944/preprints202406.1645.v1

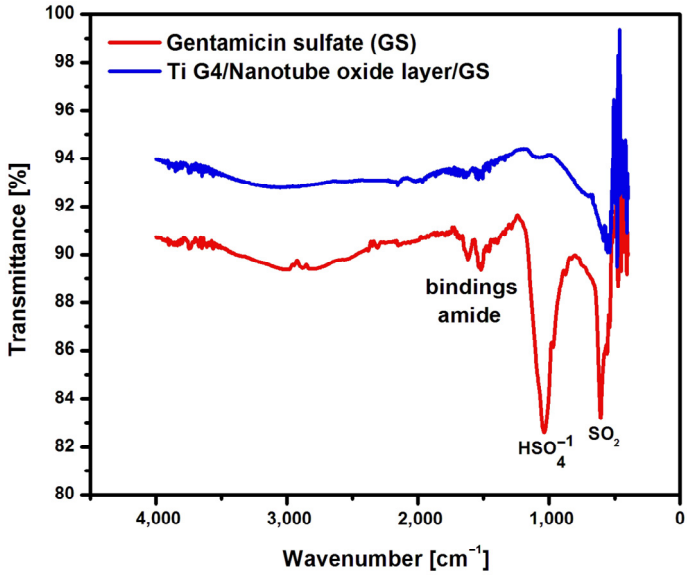

Figure 8. ATR-FTIR absorption spectrum obtained for gentamicin sulfate (GS) powder and Ti G4 sample with a layer of oxide nanotubes produced by anodization in 0.5% $AgNO_3$ solution at 80 V for 60 seconds with implemented GS.

Figure 8 shows an example ATR-FTIR absorption spectrum of gentamicin sulfate in the form of powder and the drug implemented inside the oxide nanotubes produced by anodization in 0.5% $AgNO_3$ solution at 80 V for 60 seconds. The obtained ATR-FTIR absorption spectrum shows absorption bands with wave numbers 1616, 1558 and 1456 cm^{-1}, which belong to the type I amide bond and type II amide bond present in gentamicin sulfate [38]. The peak present at 1035 cm^{-1} is related to the HSO_4^{-1} group present in the drug structure. However, the peak visible at 607 cm^{-1} is caused by the SO_2 band [39]. The ATR-FTIR absorption spectrum obtained for oxide nanotubes with the drug implemented confirms the presence of gentamicin sulfate inside the nanotubes. In the oxide nanotubes loaded with gentamicin sulfate, small amide bands are visible in the range of 1616–1456 cm^{-1} and the spectrum at 607 cm^{-1}, which proves the successful application of the drug into the interior of the fourth generation oxide nanotubes obtained on Ti G4 from an aqueous solution of 0.5% $AgNO_3$.

3.4.2. Release Kinetics of Gentamicin Sulfate from Oxide Nanotube Layers on Ti G4

Immediately after the implantation procedure, inflammation appears around the implants, which is the body's natural reaction to a foreign body in the form of an implant. Gentamicin sulfate is an antibiotic with a broad biocidal effect that can be used to extinguish inflammation. This antibiotic inhibits bacterial protein synthesis by binding to the 30S ribosomal subunit. As a result of damage to the bacterial protein membrane, irreversible changes in mRNA occur and bacterial growth is inhibited [38,40]. Gentamicin sulfate acts on Gram negative bacteria such as *Klebsiella pneumoniae*, *Escherichia coli* and gram positive bacteria such as *Staphylococcus epidermidis*, and *Staphylococcus aureus* [38]. The ability to load gentamicin sulfate into porous layers allows for localized delivery of the antibiotic directly to the site of the implant. This can help achieve high local concentrations of the drug without systemic side effects or the need for prolonged systemic antibiotic therapy. In order to determine the effect of the proposed anodization conditions, Ti G4 samples with an anodic layer of fourth-generation oxide nanotubes obtained at a voltage of 50 to 80 V for 60 seconds in 0.5% $AgNO_3$ solution and implemented gentamicin sulfate were analyzed for drug release kinetics.

Table 2 shows the amount of drug loaded inside the nanotubes depending on the voltage used in the anodic process. Based on FE-SEM images (Figure 3), it was determined that the length of the obtained nanotubes decreases as the anodizing voltage increases. The amount of gentamicin sulfate loaded correlates with the length of the oxide nanotubes. 200(16) mg of the drug penetrated into the

Preprints.org (www.preprints.org) | NOT PEER-REVIEWED | Posted: 24 June 2024 doi:10.20944/preprints202406.1645.v1

interior of the oxide nanotubes obtained at a voltage of 50 V, while for the shortest nanotubes obtained at a voltage of 80 V, 116(9) mg of gentamicin sulfate was loaded.

Table 2. The amount of gentamicin sulfate implemented inside the fourth generation oxide nanotubes on the Ti G4 surface obtained at a voltage of 50 to 80 V for 60 seconds in 0.5% $AgNO_3$ solution.

Voltage [V]	Amount of gentamicin sulfate loaded [mg]
50	200(16)
60	175(14)
70	147(12)
80	116(9)

Figure 9 shows the amount of gentamicin sulfate released from the oxide nanotube layers on Ti G4 during immersion in the PBS solution for 120 hours.

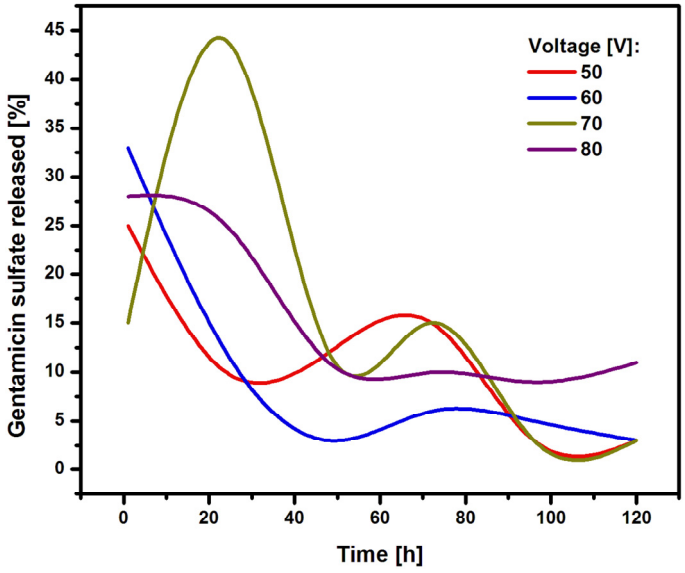

Figure 9. The amount of gentamicin sulfate released from oxide nanotube layers obtained by anodizing Ti G4 at a voltage of 50 to 80 V for 60 seconds in a 0.5% $AgNO_3$ solution.

In the first hours, the drug is intensively released from the inside of the oxide nanotubes. In the case of the longest oxide nanotubes obtained at 50 V, approximately 25% of the drug is released in the first hour. In the case of nanotubes obtained at 60 and 80 V, the initial amount of drug released was approximately 25%. Oxide nanotubes obtained at 70 V show a strong drug release from their interior of 45%. Nanotubes obtained at 50, 60 and 70 V show a dynamic course in the subsequent hours of release, with an upward trend in drug release between hours 60 and 80 of the study. Nanotubes obtained at 80 V show a constant therapeutic dose level from the 50th hour of release. This nature of drug release is related to the regular arrangement of the resulting nanotubes having a honeycomb structure. The obtained nanotubes are fully formed, which allows the drug to penetrate evenly into the nanotubes. The gentamicin sulfate is released from the interior of the oxide nanotubes in accordance with Fick's first law, which states that the amount of drug diffusing per unit time through the surface perpendicular to the direction is directly proportional to the area of this surface and the concentration gradient of the drug in the system [41].

5. Conclusions

Based on the results obtained, it can be concluded that anodizing in a 0.5% $AgNO_3$ solution in the voltage range of 50–80 V for 60 seconds is an effective and repeatable method for obtaining layers of fourth-generation oxide nanotubes on Ti G4. The obtained oxide nanotubes have a length of 1.02(2)μm at an anodizing voltage of 50 V, 550(13) nm at 60 V, 375(11) nm at 70 V, and 230(8) nm at

 doi:10.20944/preprints202406.1645.v1

80 V. An increase in anodizing voltage reduces the length of the obtained oxide nanotubes, but affects the formation of regular hexagonal nanotubes that form a honeycomb structure. During the anodizing process, silver particles are deposited on the surface of Ti G4, the presence of which was confirmed by EDS analysis. The obtained oxide nanotube layers show higher corrosion resistance compared to the Ti G4 surface not modified in ASS. The obtained fourth-generation oxide nanotubes can be a universal drug carrier in intelligent targeted drug delivery systems. The antibiotic in the form of gentamicin sulfate loaded into the obtained oxide nanotubes is released in accordance with Fick's first law. Gentamicin sulfate is dynamically released from the oxide nanotube layers obtained at 50 and 60 V, but the most effective therapeutic dose can be obtained for nanotubes obtained at 70 and 80 V. Fourth-generation oxide nanotube layers obtained under selected anodizing conditions can serve as drug carriers, which will affect to accelerate osseointegration processes and reduce post-implantation complications.

Author Contributions: Conceptualization, P.O. and B.Ł.; methodology, P.O., D.Ł., G.P. and B.Ł.; software, P.O., D.Ł. and G.P.; validation, P.O., S.S., D.Ł., G.P. and B.Ł.; formal analysis, P.O., S.S., D.Ł. and B.Ł.; investigation, P.O., S.S., D.Ł. and G.P; resources, P.O. and B.Ł.; data curation, P.O., S.S., D.Ł.and G.P; writing—original draft preparation, P.O.; writing—review and editing, S.S. and B.Ł.; visualization, P.O., S.S., D.Ł. and G.P. ; supervision, B.Ł.; project administration, P.O.; funding acquisition, P.O.

Funding: The research activities co-financed by the funds granted under the Research Excellence Initiative of the University of Silesia in Katowice.

Institutional Review Board Statement: Not applicable.

Informed Consent Statement: Not applicable.

Data Availability Statement: MDPI Research Data Policies.

Acknowledgments: The authors wish to express their gratitude to Hitachi Ltd. (Tokyo, Japan) for technical support with FE-SEM/EDS tests as part of the cooperation.

Conflicts of Interest: The authors declare no conflicts of interest.

References

1. Bhola, R.; Bhola, S.M.; Mishra, B.; Olson, D.L. Corrosion in Titanium Dental Implants/Prostheses - A Review. *Trends Biomater. Arti.f Organs* **2011**, *25*, 34–46.
2. Prasad, S.; Ehrensberger, M.; Gibson, M.P.; Kim, H.; Monaco Jr., E.A. Biomaterial Properties of Titanium in Dentistry. *J. Oral Biosci.* **2015**, *57*, 192–199. https://doi.org/10.1016/j.job.2015.08.001.
3. Batool, S.A.; Salman Maqbool, M.; Javed, M.A.; Niaz, A.; Rehman, M.A.U. A Review on the Fabrication and Characterization of Titania Nanotubes Obtained via Electrochemical Anodization. *Surfaces* **2022**, *5*, 456–480. https://doi.org/10.3390/surfaces5040033.
4. Radtke, A.; Bal, M.; Jędrzejewski, T. Novel Titania Nanocoatings Produced by Anodic Oxidation with the Use of Cyclically Changing Potential: Their Photocatalytic Activity and Biocompatibility. *Nanomater. Basel Switz.* **2018**, *8*, 712. https://doi.org/10.3390/nano8090712.
5. Fu, Y.; Mo, A. A Review on the Electrochemically Self-Organized Titania Nanotube Arrays: Synthesis, Modifications, and Biomedical Applications. *Nanoscale Res. Lett.* **2018**, *13*, 187. https://doi.org/10.1186/s11671-018-2597-z.
6. Hanif, M.B.; Thirunavukkarasu, G.K.; Liapun, V.; Makarov, H.; Gregor, M.; Roch, T.; Plecenik, T.; Hensel, K.; Sihor, M.; Monfort, O.; et al. Fluoride-Free Synthesis of Anodic TiO_2 Nanotube Layers: A Promising Environmentally Friendly Method for Efficient Photocatalysts. *Nanoscale* **2022**, *14*, 11703–11709. https://doi.org/10.1039/D2NR03379H.
7. Allam, N.K.; Grimes, C.A. Formation of Vertically Oriented TiO_2 Nanotube Arrays Using a Fluoride Free HCl Aqueous Electrolyte. *J. Phys. Chem. C* **2007**, *111*, 13028–13032. https://doi.org/10.1021/jp073924i.
8. Allam, N.; Shankar, K.; Grimes, C. Photoelectrochemical and Water Photoelectrolysis Properties of Ordered TiO_2 Nanotubes Fabricated by Ti Anodization in Fluoride-Free HCl Electrolytes. *J. Mater. Chem.* **2008**, *18*. https://doi.org/10.1039/b718580d.
9. Sreekantan, S.; Lai, Ch.W.; Lockman, Z. Extremely Fast Growth Rate of TiO_2 Nanotube Arrays in Electrochemical Bath Containing H_2O_2. *J. Electrochem. Soc.* **2011**, *158*, C397. https://doi.org/10.1149/2.020112jes.

10. Abramo, F.; Luca, F.; Passalacqua, R.; Centi, G.; Giorgianni, G.; Perathoner, S.; Abate, S. Electrocatalytic Production of Glycolic Acid via Oxalic Acid Reduction on Titania Debris Supported on a TiO_2 Nanotube Array. *J. Energy Chem.* **2021**, *68*. https://doi.org/10.1016/j.jechem.2021.12.034.
11. Moseke, C.; Lehmann, C.; Schmitz, T.; Reinert, F.; Groll, J.; Gbureck, U. Nanostructuring of Refractory Metal Surfaces by Electrochemical Oxidation: Nb and the Binary Systems Ti-Ta and Nb-Ta. *Curr. Nanosci.* **2013**, *9*, 132–138. https://doi.org/10.2174/1573413711309010022.
12. Lu, N.; Zhang, J.; Dan, Y.; Sun, M.; Gong, T.; Li, X.; Zhu, X. Growth of Porous Anodic TiO_2 in Silver Nitrate Solution without Fluoride: Evidence against the Field-Assisted Dissolution Reactions of Fluoride Ions. *Electrochem. Commun.* **2021**, *126*, 107022. https://doi.org/10.1016/j.elecom.2021.107022.
13. Wtulich, M.; Szkoda, M.; Gajowiec, G.; Jurak, K.; Trykowski, G.; Lisowska-Oleksiak, A. Hydrothermal Modification of TiO_2 Nanotubes in Water and Alkali Metal Electrolytes ($LiNO_3$, $NaNO_3$, KNO_3) – Direct Evidence for Photocatalytic Activity Enhancement. *Electrochim. Acta* **2022**, *426*, 140802. https://doi.org/10.1016/j.electacta.2022.140802.
14. Nandal, S.; Ghalaut, P.; Shekhawat, H.; Nagar, P. Osseointegration in Dental Implants: A Literature Review. *Med. Sci.* **2014**, *4*, 411–413. https://doi.org/10.15373/2249555X/July2014/129.
15. Rafieerad, A.R.; Bushroa, A.R.; Nasiri-Tabrizi, B.; Baradaran, S.; Amiri, A.; Saber-Samandari, S.; Khanahmadi, S.; Zeimaran, E.; Basirun, W.J.; Kalaiselvam, K.; et al. Simultaneous Enhanced Antibacterial and Osteoblast Cytocompatibility Performance of Ti6Al7Nb Implant by Nano-Silver/Graphene Oxide Decorated Mixed Oxide Nanotube Composite. *Surf. Coat. Technol.* **2019**, *360*, 181–195. https://doi.org/10.1016/j.surfcoat.2018.12.119.
16. Cheng, L.; Naibijiang, N.; Hasenbai, A.; Dong, H.; He, H. Bacteriostatic Effects of Nanometer Silver Disinfectant on the Biofilms in Dental Unit Water Lines. *J. Dent. Sci.* **2021**, *16*, 327–332. https://doi.org/10.1016/j.jds.2020.03.015.
17. Molly Varga Smith. *Textbook of Rabbit Medicine*, Third Edition, Elsevier Ltd., 2023, pp. 100-137. https://doi.org/10.1016/C2020-0-01089-3.
18. Smołka, A.; Rodak, K.; Dercz, G.; Dudek, K.; Łosiewicz, B. Electrochemical formation of self-organized nanotubular oxide layers on Ti13Zr13Nb alloy for biomedical applications. *Acta Phys. Pol. A* **2014**, 125(*4*), 932–935. https://doi.org/10.12693/APhysPolA.125.932.
19. Zhu, X.; Liu, L.; Song, Y.; Jia, H.; Yu, H.; Xiao, X.; Yang, X. Oxygen Bubble Mould Effect: Serrated Nanopore Formation and Porous Alumina Growth. *Monatshefte Für Chem. - Chem. Mon.* **2008**, *139*, 999–1003. https://doi.org/10.1007/s00706-008-0893-5.
20. Bauer, S.; Schmuki, P.; von der Mark, K.; Park, J. Engineering Biocompatible Implant Surfaces: Part I: Materials and Surfaces. *Prog. Mater. Sci.* **2013**, *58*, 261–326. https://doi.org/10.1016/j.pmatsci.2012.09.001.
21. Domagalski, J.T.; Xifre-Perez, E.; Marsal, L.F. Recent Advances in Nanoporous Anodic Alumina: Principles, Engineering, and Applications. *Nanomaterials* **2021**, *11*, 430. https://doi.org/10.3390/nano11020430.
22. Hang, R.; Zhao, F.; Yao, X.; Tang, B.; Chu, P.K. Self-Assembled Anodization of NiTi Alloys for Biomedical Applications. *Appl. Surf. Sci.* **2020**, *517*, 146118. https://doi.org/10.1016/j.apsusc.2020.146118.
23. Wang, K.; Liu, G.; Hoivik, N.; Johannessen, E.; Jakobsen, H. Electrochemical Engineering of Hollow Nanoarchitectures: Pulse/Step Anodization (Si, Al, Ti) and Their Applications. *Chem. Soc. Rev.* **2014**, *43*, 1476–1500. https://doi.org/10.1039/C3CS60150A.
24. Zhu, X.-F.; Song, Y.; Liu, L.; Wang, C.-Y.; Zheng, J.; Jia, H.-B.; Wang, X.-L. Electronic Currents and the Formation of Nanopores in Porous Anodic Alumina. *Nanotechnology* **2009**, *20*, 475303. https://doi.org/10.1088/0957-4484/20/47/475303.
25. Albella, J.M.; Montero, I.; Martinez-Duart, J.M. A Theory of Avalanche Breakdown during Anodic Oxidation. *Electrochimica Acta* **7**, *32*, 255–258. https://doi.org/10.1016/0013-4686(87)85032-6.
26. Masuda, H.; Fukuda, K. Ordered Metal Nanohole Arrays Made by a Two-Step Replication of Honeycomb Structures of Anodic Alumina. *Science* **1995**, *268*, 1466–1468. https://doi.org/10.1126/science.268.5216.1466.
27. Patel, Y.; Janusas, G.; Palevicius, A.; Vilkauskas, A. Development of Nanoporous AAO Membrane for Nano Filtration Using the Acoustophoresis Method. *Sensors* **2020**, *20*, 3833. https://doi.org/10.3390/s20143833.
28. Zaraska, L.; Brudzisz, A.; Wierzbicka, E.; Sulka, G.D. The Effect of Electrolyte Change on the Morphology and Degree of Nanopore Order of Porous Alumina Formed by Two-Step Anodization. *Electrochimica Acta* **2016**, *198*, 259–267. https://doi.org/10.1016/j.electacta.2016.03.050.
29. Tsuchiya, H.; Schmuki, P. Thick Self-Organized Porous Zirconium Oxide Formed in H2SO4/NH4F Electrolytes. *Electrochem. Commun.* **2004**, *6*, 1131–1134. https://doi.org/10.1016/j.elecom.2004.09.003.
30. Hossain, N.; Chowdhury, M.; Hossain, A.; Ahmed, MD.S.; Rana, Md.M.; Sultana, S. Synthesis and Characterization of Alocasia Indica Infused Silver Nanoparticles for Dental Implant Applications. *Chem. Phys. Impact* **2023**, *6*, 100239. https://doi.org/10.1016/j.chphi.2023.100239.
31. Yin, I.X.; Yu, O.Y.; Zhao, I.S.; Mei, M.L.; Li, Q.L.; Tang, J.; Chu, Ch.H. Developing Biocompatible Silver Nanoparticles Using Epigallocatechin Gallate for Dental Use. *Arch. Oral Biol.* **2019**, *102*, 106–112. https://doi.org/10.1016/j.archoralbio.2019.03.022.

32. Li, Y.; Qin, T.; Ingle, T.; Yan, J.; He, W.; Yin, J.J.; Chen, T. Differential Genotoxicity Mechanisms of Silver Nanoparticles and Silver Ions. *Arch. Toxicol.* **2017**, *91*, 509–519. https://doi.org/10.1007/s00204-016-1730-y.
33. Wassilkowska, A.; Czaplicka, A.; Zielina, M.; Bielski, A. An Analysis of the Elemental Composition of Micro-Samples Using EDS Technique. *Czasopismo Techniczne* **2014**, Chemia Zeszyt 1-Ch (18) 2014, 133-148, doi: 10.4467/2353737XCT.14.283.3371.
34. Łosiewicz, B.; Osak, P.; Maszybrocka, J.; Kubisztal, J.; Stach, S. Effect of Autoclaving Time on Corrosion Resistance of Sandblasted Ti G4 in Artificial Saliva. *Materials* **2020**, *13*, 4154. https://doi.org/10.3390/ma13184154.
35. Osak, P.; Maszybrocka, J.; Kubisztal, J.; Ratajczak, P.; Łosiewicz, B. Long-Term Assessment of the In Vitro Corrosion Resistance of Biomimetic ACP Coatings Electrodeposited from an Acetate Bath. *J. Funct. Biomater.* **2021**, *12*, 12. https://doi.org/10.3390/jfb12010012.
36. Smołka, A.; Dercz, G.; Rodak, K. Łosiewicz, B. Evaluation of corrosion resistance of nanotubular oxide layers on the Ti13Zr13Nb alloy in physiological saline solution. *Arch. Metall. Mater*. **2015**, 60(*4*), 2681–2686. https://doi.org/10.1515/amm-2015-0432.
37. Szklarska, M.; Dercz, G.; Łosiewicz, B.; Rak, J.; Simka, W. The influence of passivation type on corrosion resistance of Ti15Mo alloy in simulated body fluids. *Arch Metall Mater*. **2015**, 60(*4*), 2687–2693. https://doi.org/10.1515/amm-2015-0433.
38. Dwivedi, C.; Pandey, H.; Pandey, A.; Ramteke, P. Fabrication and Assessment of Gentamicin Loaded Electrospun Nanofibrous Scaffolds as a Quick Wound Healing Dressing Material. *Curr. Nanosci.* **2015**, *11*, 222–228. https://doi.org/10.2174/1573413710666141003221954.
39. Visan, A.; Popescu-Pelin, G.; Gherasim, O.; Grumezescu, V.; Socol, M.; Zgura, I.; Florica, C.; Popescu, R.C.; Savu, D.; Holban, A.; et al. Laser Processed Antimicrobial Nanocomposite Based on Polyaniline Grafted Lignin Loaded with Gentamicin-Functionalized Magnetite. *Polymers* **2019**, *11*, 283. https://doi.org/10.3390/polym11020283.
40. Łosiewicz, B.; Stróż, A.; Osak, P.; Maszybrocka, J.; Gerle, A.; Dudek, K.; Balin, K.; Łukowiec, D.; Gawlikowski, M.; Bogunia, S. Production, Characterization and Application of Oxide Nanotubes on Ti–6Al–7Nb Alloy as a Potential Drug Carrier. *Materials* **2021**, *14*, 6142. https://doi.org/10.3390/ma14206142.
41. Siepmann, J.; Siepmann, F. Modeling of diffusion controlled drug delivery. *J. Control. Release* **2012**, *161*(*2*), 351–362. https://doi.org/10.1016/j.jconrel.2011.10.006.